



Magnetic susceptibilities of surface sediments from estuary rivers in volcanic regions

Abd Mujahid Hamdan · Kartika Hajar Kirana · Fathul Hakim · Muhammad Iksan · Satria Bijaksana · Mariyanto Mariyanto · Teuku Muhammad Ashari · La Ode Ngkoimani · Hadi Kurniawan · Aditya Pratama · Mulyadi Abdul Wahid

Received: 27 April 2021 / Accepted: 29 January 2022 / Published online: 2 March 2022
© The Author(s), under exclusive licence to Springer Nature Switzerland AG 2022

Abstract Estuaries have very complex mechanisms because they are influenced by seawater intrusion, which causes enrichment of contaminants in the maximum turbidity area. Magnetic susceptibility measurements have been used for monitoring a wide variety of environments. However, there have been few studies of the magnetic properties of surface sediments from estuaries in volcanic environments in the tropics. This study investigates the magnetic properties and their correlations with the geochemistry of surface sediments in estuaries in volcanic areas and was conducted in the Krueng Aceh River, Indonesia. Measurements consist of magnetic susceptibility measurements, chemical analysis, and mineralogical analysis. Measurements of magnetic susceptibilities were performed using a Bartington MS2 instrument with an MS2B sensor using frequencies of 460 and 46 kHz. X-ray fluorescence (XRF)

and energy-dispersive spectroscopy (EDS) were used to identify elements in the sediments. Scanning electron microscopy (SEM) analysis was used to analyze sediment grains. X-ray diffraction (XRD) analysis was used to determine mineral contents. For the first time, χ_{LF}/χ_{FD} ratios were found to be an obvious parameter for identifying areas of sediment traps and metal enrichment in the estuary turbidity maxima (ETM) zone. The magnetic properties carried by volcanic rock minerals consist of pigeonite and enstatite. These two minerals have not been previously considered as carriers of sediments with magnetic properties when monitoring heavy metal enrichment in urban rivers. These results provide an extension of the use of magnetic susceptibility measurements in environmental studies, particularly in estuary river environments in volcanic areas such as the Krueng Aceh River, Indonesia.

A. M. Hamdan (✉) · F. Hakim · M. Iksan · T. M. Ashari · H. Kurniawan · M. A. Wahid
Faculty of Science and Technology, Universitas Islam Negeri Ar-Raniry Banda Aceh, Jl. Syekh Abdurrauf No. 1, Banda Aceh 23111, Indonesia
e-mail: mujahid@ar-raniry.ac.id

K. H. Kirana
Department of Geophysics, Faculty of Mathematics and Natural Sciences, Universitas Padjadjaran, Jl. Raya Bandung Sumedang KM.21, Bandung 45363, Indonesia

K. H. Kirana
Faculty of Mining and Petroleum Engineering, Institut Teknologi Bandung, Jalan Ganesha No. 10, Bandung 40132, Indonesia

S. Bijaksana · M. Mariyanto
Department of Geophysical Engineering, Institut Teknologi Sepuluh Nopember, Jl. Raya ITS, Surabaya 60111, Indonesia

L. O. Ngkoimani
Department of Geophysics, Halu Oleo University, Indonesia, Kampus Hijau Bumi Tridharma, Kendari 93232, Indonesia

A. Pratama
Research Center for Geotechnology, JL. Sangkuriang, Indonesian Institute of Sciences (LIPI), Kompleks LIPI, Bandung 40135, Indonesia

Keywords Estuary · Volcanic · Magnetic susceptibility · Monitoring, river · Heavy metals

Introduction

Estuaries are intermediate areas of freshwater and marine environments that are prone to pollution by organic and inorganic contaminants. Rivers have attracted the attention of researchers in recent years (Peter et al., 2020; Xu et al., 2020) due to their complex mechanisms for various processes, such as hydrodynamics, sediment dynamics, metal enrichment, and processes involving organic matter. Due to these mechanisms, the environmental quality of estuaries is very susceptible to decline. This is particularly true if the river estuary is in an urban industrial area (De Souza Machado et al., 2016).

Environmental monitoring is needed as a basis for preventing changes and negative impacts on the sustainability of living things and their ecosystems (Chandrasekaran et al., 2020; Kumari et al., 2020). The choice of effective and efficient technology is an essential factor in successful monitoring. Several approaches have been used in monitoring, including biological, chemical, and physical approaches (Artiola & Brusseau, 2019). Environmental monitoring using magnetic susceptibility measurements is one method that has been used extensively to monitor the environments of various regional objects such as lakes (Yunginger et al., 2018), rivers (Jin et al., 2019; Mariyanto et al., 2019; Sudarningsih et al., 2017; Togibasa et al., 2018), and the sea (Li et al., 2020). Objects that can be analyzed include sediments (Yunginger et al., 2018), rock (Reyes et al., 2013), soils (Kanu et al., 2014; Novala et al., 2016), and plants (Hamdan et al., 2019, 2020). For sediments, magnetic susceptibility measurements have been carried out in environmental monitoring, such as with topsoil (Reyes et al., 2013), lake sediments (Bao et al., 2011; Yunginger et al., 2018), marine sediments, and river sediments (Mariyanto et al., 2019; Sudarningsih et al., 2017).

However, the magnetic properties of estuarine river sediments in volcanic environments have not been studied before. It is assumed that metal enrichment in estuaries is more complex than that in freshwater rivers. This is because metal enrichment in an estuary area is influenced by many factors, such as salinity, hydrodynamics, the entry of marine elements, and the influence of biogeochemistry in the riverbed (Chen et al., 2001; Dessai et al., 2009; Priya

et al., 2016; Reitermajer et al., 2011; Wu et al., 2012). The presence of the estuary turbidity maxima (ETM) zone in the estuary river allows magnetic sediment to be trapped in the turbidity region. Furthermore, heavy metal enrichment occurs in turbidite areas due to biological, chemical, and physical mechanisms. Thus, in ETM zones in volcanic areas, heavy metal enrichment is thought to be related to the abundance of magnetic sediments in the river (De Souza Machado et al., 2016).

This study is designed to identify the relationship between magnetic susceptibility and geochemistry of surface sediments of the Krueng Aceh River as a pilot project for monitoring the environmental quality of the river and its surrounding areas. This river was chosen because it is located in a volcanic complex with massive sediment transport from surrounding alluvium formations (Bennett et al., 1983). It is hypothesized that the presence of magnetic minerals in the sediments will be a source of magnetization and can be used as a proxy for metal enrichment and ETM zones. Another reason for choosing the Krueng Aceh River is because this river is located in a medium-sized urban area where metal enrichment is not affected by massive anthropogenic materials such as rivers in metropolitan industrial areas but most likely from a lithogenic process; this means that the analysis can be limited to correlations of magnetic susceptibility, metal enrichment, and other mechanisms at the estuary.

Materials and methods

The Krueng Aceh River is located in the Aceh Besar District and Banda Aceh City, as shown in Fig. 1. The Krueng Aceh River is a river that empties into the Strait of Malacca, which is an estuary area in the north section of the river. The Krueng Aceh River has a length of approximately 145 km and passes through the Krueng Aceh Basin or Valley (Moechtar et al., 2009). This river is a source of clean water and irrigation for the community. According to Bennett et al. (1983), Krueng Aceh rock formations are distinguished by quaternary, tertiary, and pretertiary rock formations. These rock types are classified as surface sedimentary rock, sedimentary rock, metamorphic rock, or volcanic rock. Sedimentary rocks consist of sandstones, tuffaceous sandstones, limestone

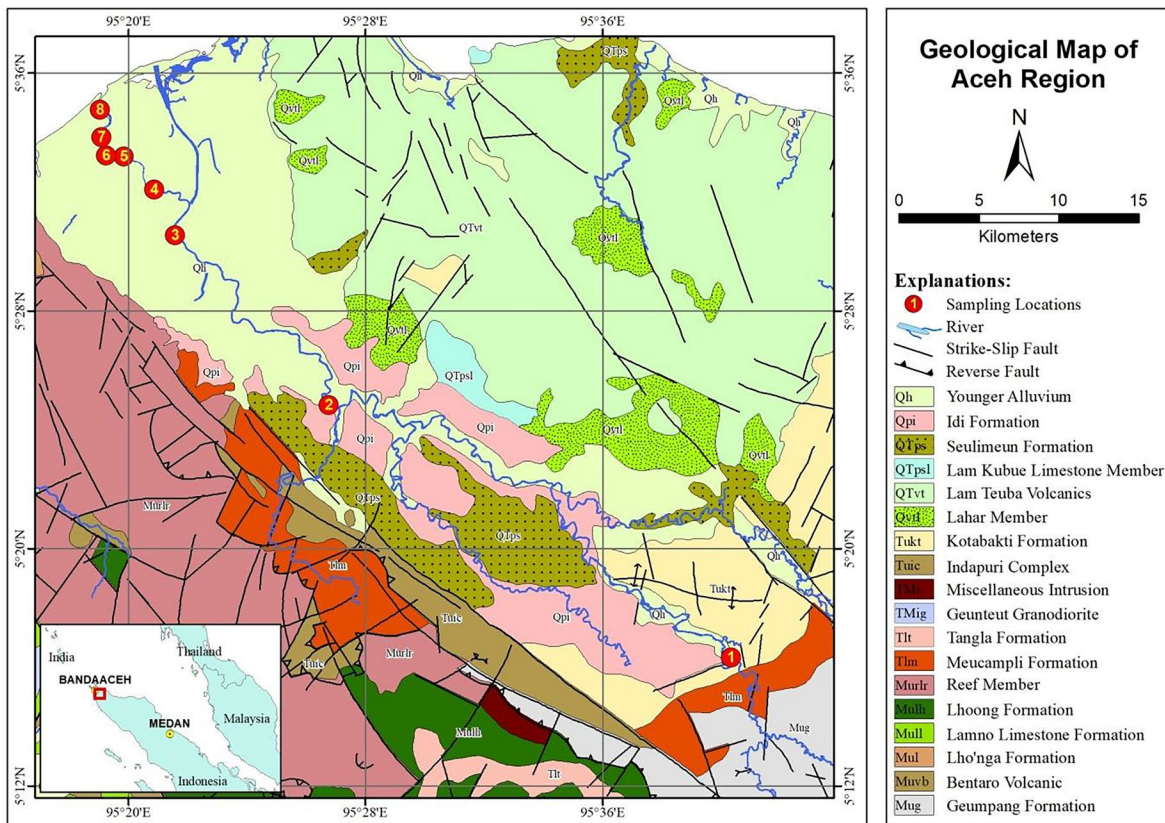


Fig. 1 Geological map of the study area shows the sampling sites along the Krueng Aceh River (red dots) (modified from Bennett et al., 1983)

sandstones, conglomerates, tuff sandstones, shale, and limestone. Metamorphic rocks consist of phyllite, slate, and marble. Additionally, the quaternary and tertiary volcanic arrangements consist of ash, tuff, lava, agglomerates, breccias, pumice breccias, lava flows, and lava (which are andesite to dacite and andesite to basalt and granodiorite) and ultramafic intrusion rocks.

Sampling points are shown as eight points in the midstream of the river in Fig. 1. Sediment samples were collected using a sediment grabber at the bottom of the Krueng Aceh River and were stored in plastic containers. Samples were collected in November 2019. The sediment grabber was lowered to the riverbed using a rope. Methods of sample preparation followed the procedure of Mariyanto et al. (2019). The samples were first sieved using a 40 mesh sieve, placed on plastic trays and air-dried at room temperature. The process at this stage produced bulk samples.

A small portion of dried bulk samples was then mixed with 250 ml distilled water in a beaker for magnetic extraction. Hence, the raw samples were extracted by the mechanical magnetic extraction technique. The extraction was carried out by removing a magnetic stirrer dipped in the solution every 5 min until no magnetic minerals could be drawn. The extraction was carried out manually with a weak magnet to extract only strongly magnetic minerals (see Togibasa et al., 2018). The extracted grains were then pulverized and sieved using a 200 mesh sieve. Water samples were collected using grab water sampling.

Magnetic susceptibility measurements were carried out on bulk samples using a Bartington MS2 instrument with an MS2B sensor that operates at two frequencies, i.e., 470 Hz and 4.7 kHz. The measurements with these two sensors produced low-frequency mass-based magnetic susceptibility (χ_{LF}) and its high-frequency counterpart (χ_{HF}). The frequency-dependent magnetic

susceptibility ($\chi_{FD}(\%)$) could then be calculated from $\chi_{FD}(\%) = \left(\frac{\chi_{LF} - \chi_{HF}}{\chi_{LF}} \right) \times 100\%$.

Metal content was determined by using X-ray fluorescence (XRF) analysis. The bulk sample was prepared using a pellet press. XRF analysis was performed using a PANalytical AXIOS X-ray fluorescence instrument. The extracted sample was analyzed for mineralogy using X-ray diffraction (XRD) with the Rigaku-SmartLab X-ray diffractometer instrument. Morphological observations of the extracted samples were carried out by scanning electron microscopy-energy-dispersive spectroscopy (SEM-EDS) analysis using a JED-2300 T energy-dispersive X-ray spectrometer. The geoaccumulation index (I_{geo}) was calculated by $I_{geo} = \ln\left(\frac{C_n}{1.5B_n}\right)$, where C_n is the metal concentration at the sampling point and B_n is the metal concentration at the background point. B_n is a point on the absence of anthropogenic activity (Haris et al., 2017), and it is station 1 in Fig. 1. Correlation analyses used Pearson’s correlation (Hamdan et al., 2020). The turbidity of water was determined by a turbidity meter (Amtast Amt21).

Results

XRF analysis results and water turbidities are shown in Table 1. The highest turbidity value was found at point 5, and the lowest turbidity was at point 1. Metal concentrations indicated that each sediment sample contained Cr, Ti, Mn, Fe, Zn, Ni, Mg, Al, Si, Ca, and Sr, and samples from points 2 and 8 also contained Cu. Table 1 shows different patterns of concentration

Table 2 Heavy metal geoaccumulation indexes. In italics are polluted states

Sampling point	Geoaccumulation index				
	Cr	Ni	Fe	Zn	Mn
1	-0.41	-0.41	-0.41	-0.41	-0.41
2	-0.57	-0.20	-0.27	-0.22	-0.21
3	-0.75	-0.42	-0.52	-0.28	-0.42
4	-1.30	-0.12	-0.45	-0.36	-0.48
5	<i>0.30</i>	-0.29	-0.22	-0.24	-0.45
6	-0.58	0.00	-0.28	<i>0.10</i>	-0.69
7	-0.41	<i>0.13</i>	-0.23	<i>0.08</i>	-0.52
8	-1.17	<i>0.15</i>	-0.19	<i>0.35</i>	-0.44

changes for each element in eight sampling locations. This indicates the complexity of metal enrichment mechanisms in river sediments. Except for Mn and Mg, each element exhibited a significant change at point 5 compared to point 4.

Analyses of geoaccumulation indexes are shown in Table 2. Geoaccumulation indexes show that the points 5 are polluted by Cr. The concentration of Fe in the sample is relatively high compared to results from several measurements in nonvolcanic rivers (Mariyanto et al., 2019; Naseh et al., 2012); however, based on the geoaccumulation index, no river point was polluted by Fe. The Zn content increased from points 6 to 8 in the lightly polluted category. Likewise, the Ni content increased from point 7 to point 8 in the lightly polluted category.

Table 3 shows the results of measurements of low frequency (χ_{LF}), high frequency (χ_{HF}), and frequency-dependent magnetic susceptibility (χ_{FD}). The

Table 1 Metal concentrations in the sediment samples and water turbidity from the Krueng Aceh River. –, below the detection limit

Sampling points	Metal concentration (mg/kg)												Turbidity (NTU)
	Cr	Ti	Mn	Fe $\times 10^3$	Zn	Ni	Mg $\times 10^2$	Al $\times 10^3$	Si $\times 10^3$	Ca $\times 10^3$	Cu	Sr	
1	1120	10,600	2820	135	209	340	397	134	512	94.7	-	1510	1.51 ± 0.29
2	950	13,100	3440	155	251	418	242	163	522	57.2	296	1250	1.40 ± 0.11
3	790	9660	2780	120	237	336	264	133	553	79.6	-	1340	3.24 ± 0.12
4	460	10,200	2610	129	218	451	248	150	546	66.0	-	1330	10.26 ± 0.44
5	2260	17,300	2690	163	246	381	286	138	491	87.7	-	1240	28.40 ± 0.86
6	940	12,700	2120	153	345	0	264	155	501	78.6	-	1210	20.00 ± 0.91
7	1110	12,400	2510	161	338	578	264	173	509	48.5	-	997	18.20 ± 0.63
8	521	11,900	2720	167	447	593	263	176	473	38.8	341	943	9.45 ± 0.71

Table 3 Magnetic susceptibility measurement data for sediment samples from the Krueng Aceh River. χ_{LF} is low-frequency magnetic susceptibility, χ_{HF} is high-frequency magnetic susceptibility, and χ_{FD} is frequency-dependent magnetic susceptibility

Sample code	χ_{LF} ($\times 10^{-6} \text{ m}^3 \cdot \text{kg}^{-1}$)	χ_{HF} ($\times 10^{-6} \text{ m}^3 \cdot \text{kg}^{-1}$)	χ_{FD} (%)
1	706.3 \pm 1.2	705.8 \pm 1.4	0.07
2	389.6 \pm 2.4	385.5 \pm 2.8	1.05
3	603.2 \pm 3.7	597.4 \pm 2.6	0.96
4	428.3 \pm 2.5	412.8 \pm 3.7	3.62
5	1385.9 \pm 11.6	1385.4 \pm 14.1	0.03
6	1184.3 \pm 17.5	1173.9 \pm 25.9	0.88
7	258.1 \pm 3.4	248.6 \pm 7.6	3.68
8	95.7 \pm 0.2	89.2 \pm 1.7	6.79

results of these analyses indicate that there are differences in the values at each sampling point. Based on the data in Table 3, point 5 was the point with the highest susceptibility value and was increased drastically compared to point 4. The value of χ_{FD} also changed drastically at point 5 compared to point 4.

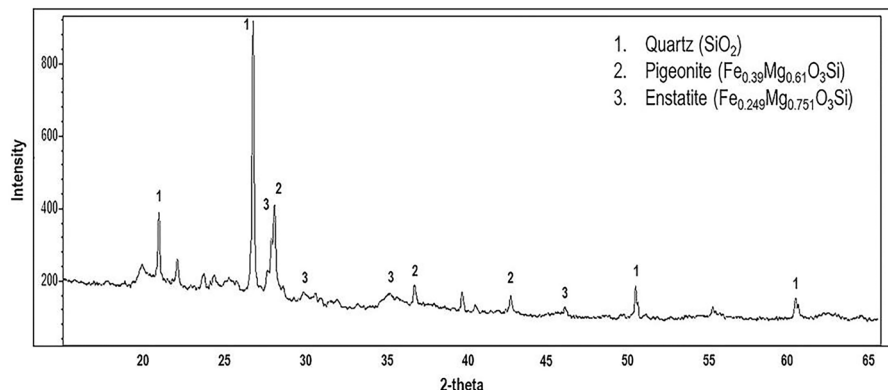
The results of XRD analyses are shown in Fig. 2. The diffractogram shows that the minerals in the extraction sample consist of quartz, pigeonite, and enstatite. Strongly ferromagnetic minerals such as magnetite and hematite were not found in the analyzed samples. The results of SEM–EDS analysis are shown in Fig. 3. These results support conclusions drawn from mineralogical analyses of the XRD diffractogram, and they show the presence of Mg, Si, Fe, and O elements in the sediment. These elements make up the minerals quartz, pigeonite, and enstatite.

Discussion

Based on the turbidity data in Table 1, point 5 is the point with the highest turbidity. This indicates that the point is in the ETM zone. The concentrations of

Al, Fe, Zn, and Ni tended to increase toward the estuary zone from point 5. Additionally, the concentrations of Ti, Mg, Ca, and Cr tended to decrease toward the estuary zone. The concentrations of elements such as K, Na, and Mg were found to be very high in the upstream area of the river. Concentrations of Cu were only found at points 2 and 8. Metal in the river may come from geological weathering and the discharge of agricultural, residential, and waste products (Chen et al., 2001). Metal distributions in surface sediment are determined by speciation, precipitation, solubilization, diffusion, and advection mechanisms. All of these processes can occur in the form of physical, chemical, and biological processes that operate in the water column (Dessai et al., 2009; Moechtar et al., 2009 & De Souza Machado et al., 2016). Metal enrichment in sediments is determined by several parameters, such as the effects of tides, freshwater discharge, waves, winds, topography of the estuary, sediment particle size, salinity, river discharge, local currents, suspended sediment concentration, oxygen level, and pH (Chen et al., 2001; Dessai et al., 2009; Priya et al., 2016; Reitermajer et al., 2011; Wu et al., 2012).

Fig. 2 XRD diffractogram for sediment taken from point 8



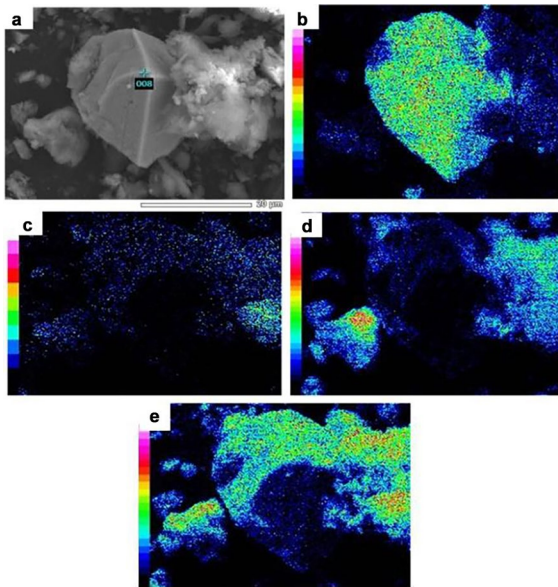


Fig. 3 SEM–EDS observation of **a** extracted sediment; **b** iron (Fe); **c** magnesium (Mg); **d** silicon (Si); and **e** oxygen (O)

Based on Table 1, crustal metals such as Ti, Al, Si, and Fe have different properties in downstream areas. The downstream section of the river has increased water salinity (Adib & Javdan, 2015). The gradient for metal enrichment was also strongly influenced by physicochemical properties in the estuary region. One of the most influential parameters is salinity. Salinity affects sediment flow, concentration and partitioning, sedimentation and metal removal from surface water, and metal remobilization processes. Metals within sediments in estuarine regions are attributed to either conservative or nonconservative behaviors of metals. Conservative behavior causes metal concentrations to decrease linearly with increasing salinity (De Souza Machado et al., 2016). Therefore, Ti is conservative with respect to salinity; on the other hand, Fe and Al are not conservative (Chu et al., 2014; De Souza Machado et al., 2016). Fe in the sediments is probably dominated by Fe from geological weathering sediments (Esteller et al., 2017). Moreover, the abundance of Si in sediments is probably influenced by the flow of Si from marine environments into the river and/or due to the geological setting of the river in the alluvium area. The presence of Si in river sediments needs further research to understand its mechanisms for pedogenesis, solubility,

granulometry, and deposition (Fabre et al., 2019; Nakanishi et al., 2019).

Figure 4 shows the correlation of Fe, Mn, and Ca levels with those of the other elements for points 5 to 8. Based on the data in Fig. 4, Mn and Fe levels exhibit a significant correlation ($R=0.97$) in the area suspected of being the estuary zone. Apart from the presence of the same bedrock, this is suspected to be because Fe and Mn undergo similar adsorption, coagulation, flocculation, and precipitation processes (Oldham et al., 2017). The increase in Fe and Mn concentrations at point 5 can be caused by adsorption and the abundance of suspended organic particles that adsorb Fe and Mn and the flocculation process caused by seawater intrusion (Zhu et al., 2018). According to Jilbert et al. (2018), Fe enters the estuary area as a mixture of Fe oxyhydroxides with dissolved organic matter (DOM). Then, a flocculation of Fe and partial decoupling from DOM give ferrihydrite and Fe(III)-organic matter. The abundance of Fe/Mn at point 6 was decreased compared to point 5, which is thought to be due to Fe/Mn complexation by ligands in the water column. From point 6 to point 8, the concentrations of Fe and Mn in the sediment tended to increase. In areas with high salinity levels, there is competition for ligand complexation between Fe/Mn ions and marine ions, especially Ca^{2+} and Mg^{2+} (Hopwood et al., 2015). Furthermore, Fe–Mn oxides in sediments absorb or precipitate metals in water bodies (De Souza Machado et al., 2016).

Figure 4 also shows that Fe and Mn concentrations in the sediment correlated with Ni concentrations in the sediment. Furthermore, the concentrations of Fe and Mn showed a significant negative correlation with Sr level and a positive correlation with Ca level. This is presumably because Sr is an element originating from the ocean and is possibly derived from calcic biota (Zhao et al., 2016). Additionally, Cr concentration has a positive correlation with Ca concentration, which indicates that most of the Cr is likely to have been precipitated in the form of carbonate. However, Ni and Zn concentrations were negatively correlated with Ca concentrations. This is probably because calcium carbonate acted as a diluent of the clay fraction (Kowalska et al., 2021).

Table 1 shows that Ni and Zn were identified at an upstream point. This indicates that Ni and Zn were present in the sediment as lithogenic products because in the upstream area, there is no contamination from

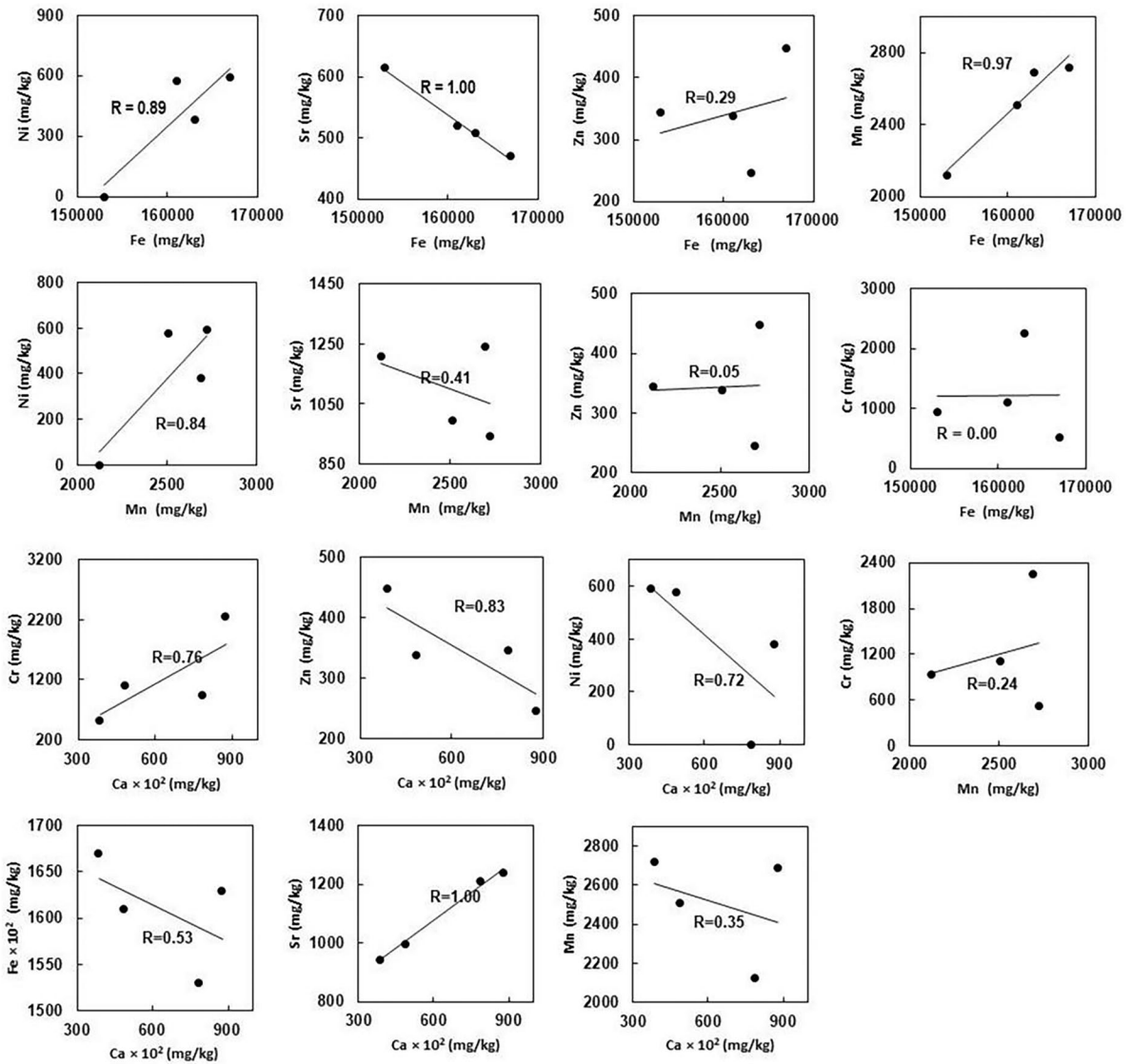
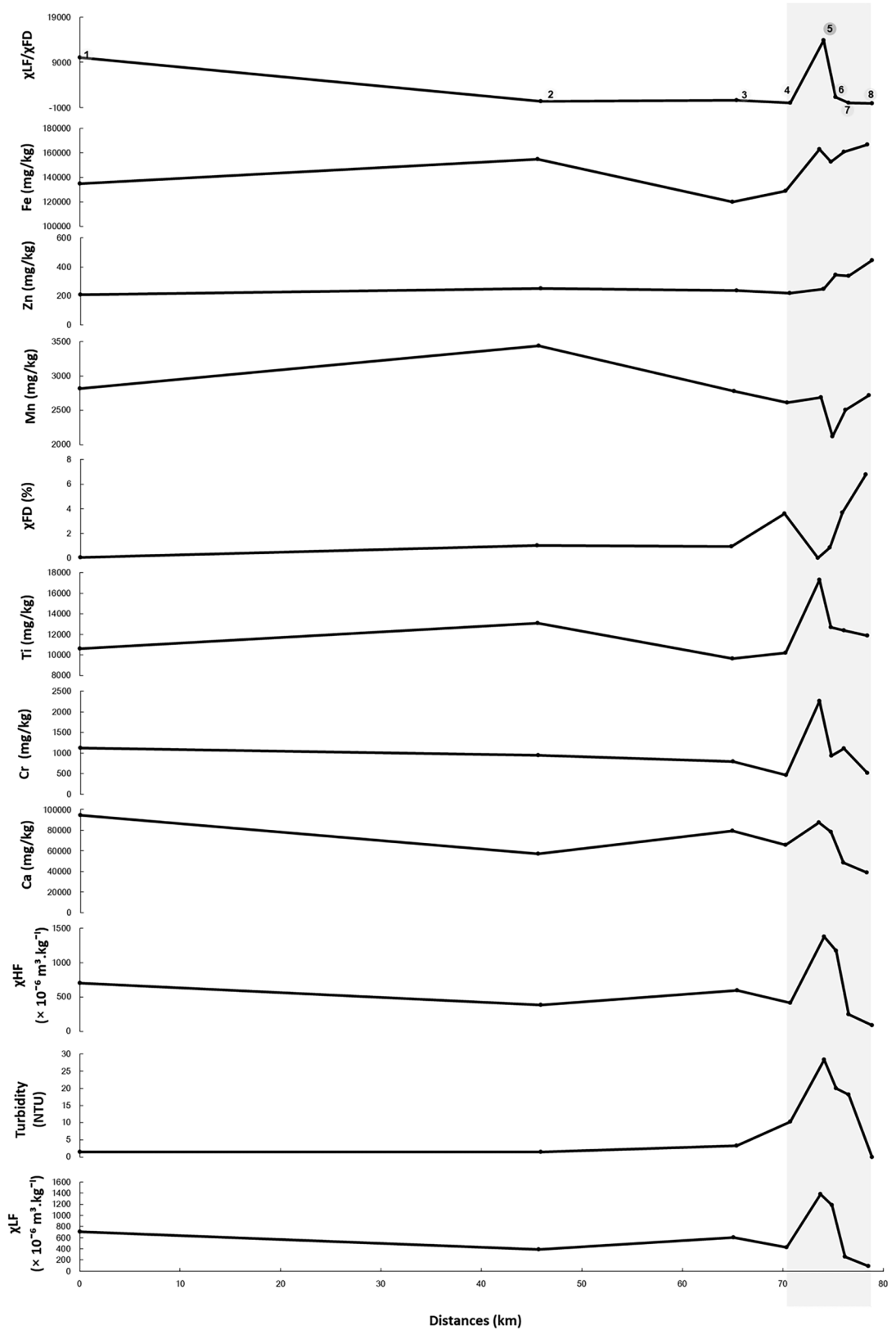


Fig. 4 Correlation between metal concentrations in sediment samples from the Krueng Aceh River

anthropogenic activity. The concentrations of Zn and Ni are linearly related to salinity, which indicates that these metals are not conservative (Chu et al., 2014; De Souza Machado et al., 2016). The metal enrichments from points 5 to 8 indicate that this point is an ETM zone (De Souza Machado et al., 2016). ETM are influenced by hydrodynamic factors, sediment dynamics, and transport of suspended particulate matter (Burchard et al., 2018). The particles or colloids in the ETM zone then affect the mobilization, adsorption, and precipitation of metals. In this zone,

metal enrichment in sediments tends to occur through the interaction of surface forces (De Souza Machado et al., 2016). Furthermore, it is also possible that the enrichment of Zn and Ni comes from ions originating in the water column (Meng et al., 2008; Yang et al., 2012; Yi et al., 2012).

Based on Table 1, the increased concentrations of Zn and Ni probably originated from anthropogenic sources in the form of dissolved ions and accumulations of sediments containing both metals. Zn can come from various sources, including electronic wastes, road surfaces,



◀**Fig. 5** Distributions of the χ_{LF} , χ_{FD} , and χ_{LF}/χ_{FD} values and metal concentrations along the Krueng Aceh River from downstream (0 km) to upstream (80 km)

dissolved Zn from corrosive community roofs, and agricultural pesticides (Fujimori & Takigami, 2013). Anthropogenic sources of Ni metal include waste steel and materials used in construction activities (Kumar et al., 1994). The presence of Cu at point 2 is thought to have originated from rock mining activities that contaminated river tributaries that entered the river before point 2. However, the abundance of Cu at point 8 is thought to result from accumulation of Cu that was flocculated due to increased salinity.

Changes in the values of χ_{LF} and χ_{FD} from point to point are shown in Fig. 5. Changes in the values of χ_{LF} and χ_{FD} from points 3 to 8 were not caused by geological factors involving changes in rock formations. This is shown in Fig. 1, which shows that these points are located within the same geological formation. The points are in the alluvium formation, which consists of clastic sediments. Point 5 is suspected to be a transition area for metal enrichment, where χ_{LF} and χ_{FD} values change significantly compared to those at the previous point. The increasing value of χ_{LF} indicates the abundance of magnetic minerals at that point. The low χ_{FD} value at point 5 indicates that the abundance of magnetic minerals arises from particles in the suspended multidomain size. Denser magnetic minerals are likely trapped at this point. However, lighter magnetic minerals are transported downstream (Badesab et al., 2012).

Based on Fig. 5, point 1 and point 5 exhibited higher χ_{LF}/χ_{FD} values than the other points. At point 5, the value of χ_{LF}/χ_{FD} also increased with a very extreme gradient. The high χ_{LF}/χ_{FD} at point 1 was caused by the sample analyzed, which was dominated by sediments that did not change in size due to transport dynamics. The high value of χ_{LF}/χ_{FD} at point 5 probably arose because the point is in a large magnetic sediment trap area. This shows that a comparison of χ_{LF}/χ_{FD} values can provide qualitative information on points that have magnetic minerals with larger sizes and high magnetization. To prove this supposition, a granulometric analysis and a mineralogy study are needed at that point.

Based on the results of the Pearson correlation analysis shown in Table 4, the values of χ_{LF} were correlated significantly with the concentration of Cr.

Although not significant, the values of χ_{LF} were also linearly correlated with the concentrations of Ca, Mg, and Ti. However, assuming that points 5 to 8 are estuary regions, correlations between χ_{LF} values and element concentrations were expected, and this is shown in Fig. 6. The figure shows correlations between the values of χ_{LF} and the concentrations of Fe, Ca, Ti, Ni, Cr, Zn, Sr, Mg, Al, and Si. Figure 6 shows the pattern of χ_{LF} values with several elements. The results of correlation analyses show that the value of χ_{LF} has a significant linear correlation with the concentration of Ca. It is suspected that there are ferromagnetic minerals with strongly magnetic Ca-based or carbonate-based minerals in the estuary area. The linear correlation between the χ_{LF} value and the concentration of Ti is probably due to Ti-based magnetic minerals, which can also be found in sediments resulting from weathering of volcanic rock. However, it is possible that Ca association with magnetic minerals is caused by biogeochemical processes of microorganisms (Monteil et al., 2020).

The increase in χ_{LF} at point 5 is probably due to the abundance of Fe-based magnetic minerals. This is supported by the increase in the concentration of Fe at that point. However, based on Table 4, the χ_{LF} value did not show a significant correlation with the concentration of Fe. This result differs from previous reports in that the χ_{LF} values of river sediments were always correlated with the concentration of Fe (Naseh et al., 2012). The difference in χ_{LF} values for sediments generally comes from differences in the type and abundance of magnetic minerals within each sample. The value of χ_{LF} is generally driven by Fe-based minerals, so changes are very sensitive to Fe abundance (Canbay et al., 2010; Mariyanto et al., 2019; Sudarningsih et al., 2017).

Based on the XRD analysis, the minerals in the extraction samples consisted of quartz, pigeonite, and enstatite. The results showed that strongly ferromagnetic minerals such as magnetite and hematite were not found in the analyzed samples. Strongly magnetic Fe-oxide minerals are likely trapped in the area around point 5. Quartz, pigeonite, and enstatite are minerals originating from volcanic lava in the mafic region and ultramafic igneous rock (Biedermann et al., 2015). The presence of these minerals in the sediment is probably caused by the dynamics of sedimentation in the estuary area. SEM observations confirmed that magnetic minerals are lithogenic particles

Table 4 Pearson correlation between magnetic parameters and heavy metal contents. *R* values for strong correlation (> 0.707 , $n=8$, $p=0.5$) are in italics

	Cr	Ni	Zn	Ti	Fe	Mn	Si	Al	Mg	Ca	χ_{LF}	χ_{FD}
Cr	1.00											
Ni	-0.33	1.00										
Zn	-0.27	<i>0.87</i>	1.00									
Ti	<i>0.85</i>	0.04	0.10	1.00								
Fe	0.37	0.64	0.68	<i>0.72</i>	1.00							
Mn	-0.00	-0.32	-0.35	0.01	-0.05	1.00						
Si	-0.34	-0.52	-0.71	-0.60	-0.88	0.20	1.00					
Al	-0.37	<i>0.93</i>	<i>0.79</i>	0.06	0.70	-0.01	-0.47	1.00				
Mg	0.27	-0.44	-0.33	-0.11	-0.21	0.00	-0.15	-0.51	1.00			
Ca	0.50	-0.91	-0.70	0.10	-0.49	-0.14	0.26	-0.93	0.61	1.00		
χ_{LF}	<i>0.72</i>	-0.67	-0.33	0.58	0.02	-0.37	-0.13	-0.61	0.23	0.79	1.00	
χ_{FD}	-0.59	<i>0.89</i>	<i>0.73</i>	-0.26	0.33	-0.12	-0.31	<i>0.76</i>	-0.40	-0.87	-0.75	1.00

characterized by grain morphologies that are not spherical (Labrada-Delgado et al., 2012). However, further mineralogical analysis is required for samples from the ETM zone.

Theoretically, χ_{FD} values indicate superparamagnetic abundance (Kanu et al., 2014). Based on Fig. 5,

the values of χ_{FD} were $< 2\%$ in the upstream areas (points 1 to 3), which indicates a low superparamagnetic abundance; it can also be interpreted to indicate multidomain grain sizes (Dearing, 1999). This is very logical because the sediments in the upstream area have not changed their shapes and sizes into

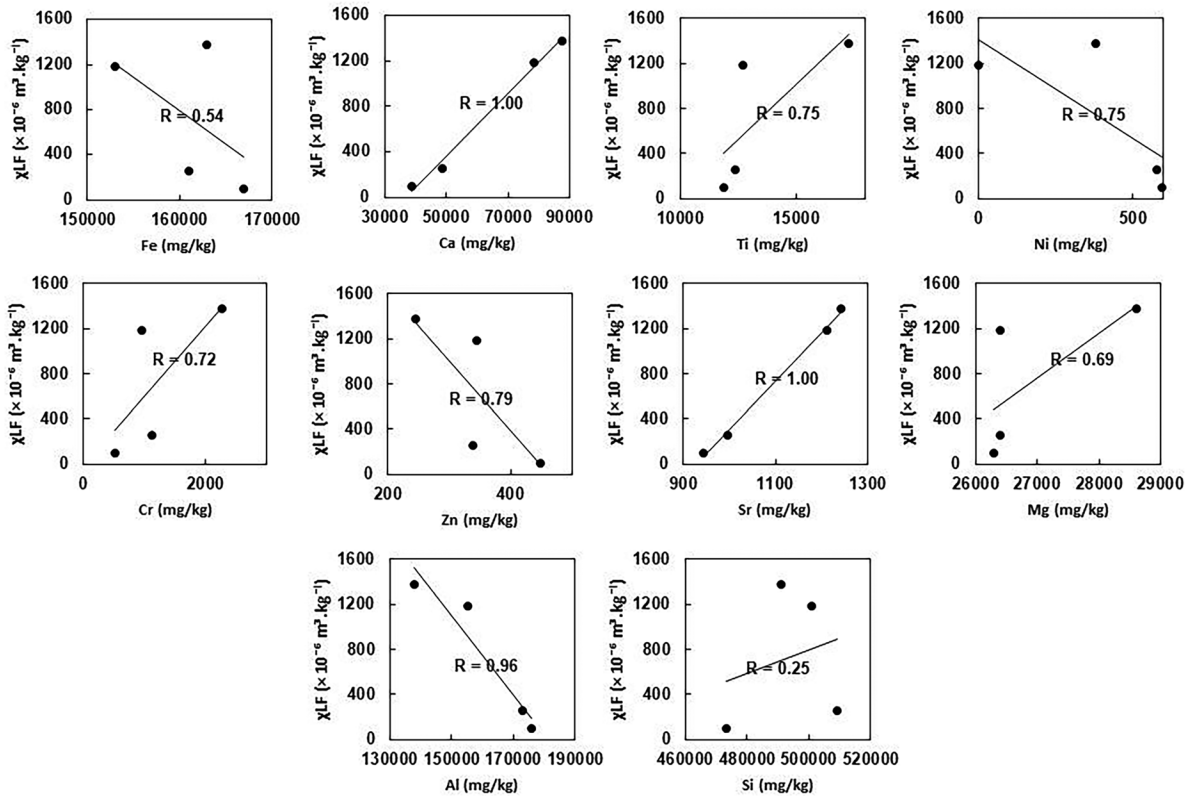


Fig. 6 Correlation between χ_{LF} values and the metal concentrations at points 5 to 8

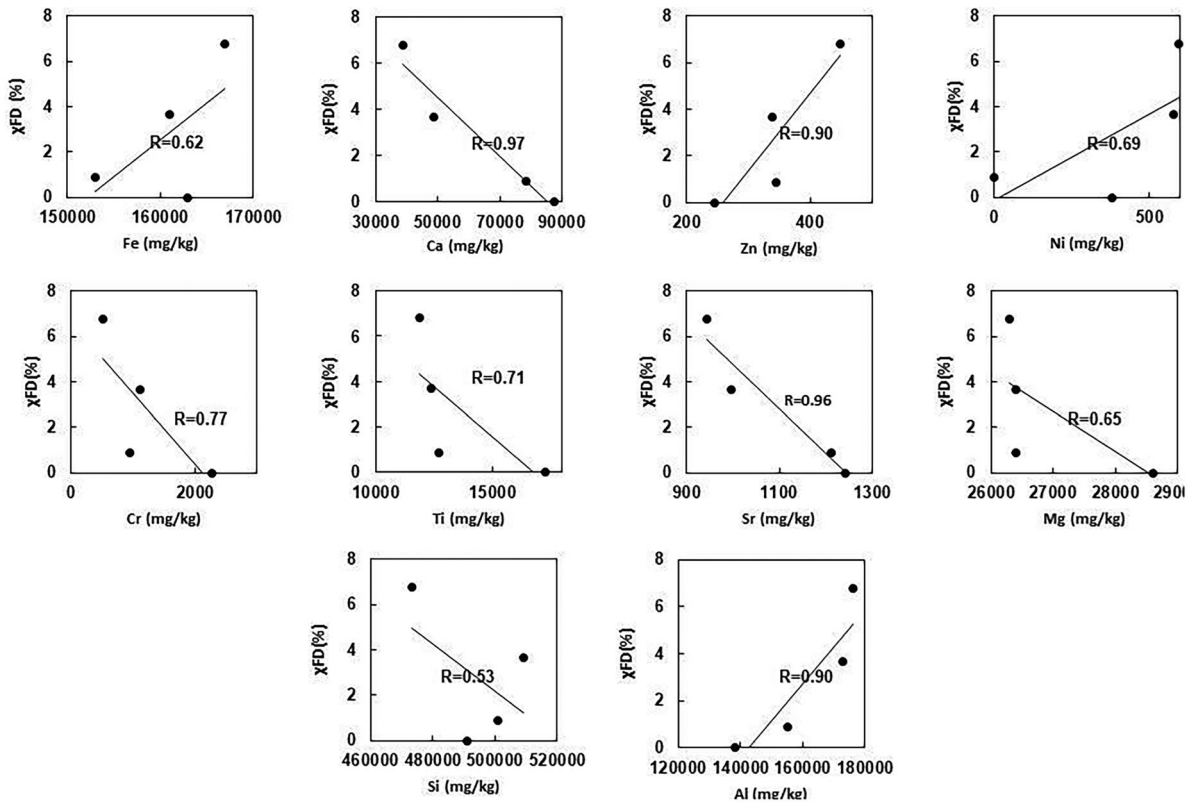


Fig. 7 Correlations between χ_{FD} values and metal concentrations at points 5 to 8

small and fine grains due to physical processes such as transport and weathering (Ananthapadmanabha et al., 2014). Based on the previous discussion, point 5 is considered to be in the ETM zone. The value of χ_{FD} was less than 2% at this point, and this is thought to be due to the abundance of organic matter particles, which are more dominant than superparamagnetic minerals. However, at points 4, 7, and 8, the values of χ_{FD} were $2\% < \chi_{FD} < 10\%$, which indicates that there was superparamagnetic grain enrichment at these points. The abundance of superparamagnetic grains may have resulted from weathering of bedrock and anthropogenic particles. The weathering of rocks is determined by regional climates. In tropical areas, weathering is more prevalent than it is in other climates (Ananthapadmanabha et al., 2014).

It is possible that the presence of superparamagnetic grains as anthropogenic particulates comes from shipping, waste disposal, and land use around points 7 and 8, which are near a traditional market. Based on the Pearson correlation matrix shown in Table 4, the χ_{FD}

values exhibited a significant negative correlation with Ca concentration. This is suspected of forming Ca-based magnetic minerals or those associated with Ca in the estuary, and these comprise a multidomain or single domain and are not in a superparamagnetic form. Based on Fig. 7, χ_{FD} values exhibited a tendency to increase with increasing concentrations of Fe, Zn Al, and Ni, although these trends were not significant. The presence of Zn and Ni in the sediment could also be due to the Fe oxide precipitation mechanism mentioned earlier. However, the χ_{FD} value showed negative correlations with the concentrations of Sr and Mg. These two metals probably arise from marine environments together with Ca, and their mechanisms result from their association with carbonate-based minerals.

Conclusion

The values of χ_{LF} , χ_{FD} , and χ_{LF}/χ_{FD} can be proxy indicators identifying ETM and heavy metal enrichment zones. The values of χ_{LF}/χ_{FD} increased sharply at

points suspected of being sediment traps in the ETM zone. The parameter χ_{LF}/χ_{FD} has never been used as a proxy parameter to identify the ETM zone. Thus, these results expand the use of magnetic susceptibility parameters in monitoring river environments, especially in estuary rivers in volcanic environments.

χ_{LF} values increased, possibly due to enrichment of magnetic minerals at points of maximum turbidity due to mechanisms of magnetic sediment dynamics and/or chemical and biological processes. On the other hand, χ_{FD} values decreased drastically in the turbidity zone due to the low abundance of superparamagnetic minerals. Thus, magnetic susceptibility analysis constitutes a new supplemental method for identifying ETM zones. Unlike metropolitan or industrial areas, the Krueng Aceh estuary river, which is in a volcanic area and is surrounded by a geological formation in the form of alluvium, contains pyroxene minerals consisting of pigeonite and enstatite that serve as carriers of magnetic minerals. Further mineralogical analysis is needed to analyze magnetic minerals in the maximal turbidity area.

Data availability Source data for figures are provided with the paper.

Declarations

Conflict of Interest The authors did not receive support from any organization for the submitted work. All authors certify that they have no affiliations with or involvement in any organization or entity with any financial interest or non-financial interest in the subject matter or materials discussed in this manuscript.

References

- Adib, A., & Javdan, F. (2015). Interactive approach for determination of salinity concentration in tidal rivers (Case study: The Karun River in Iran). *Ain Shams Engineering Journal*, 6(3), 785–793. <https://doi.org/10.1016/j.asej.2015.02.005>
- Ananthapadmanabha, A. L., Shankar, R., & Sandeep, K. (2014). Rock magnetic properties of lateritic soil profiles from southern India: Evidence for pedogenic processes. *Journal of Applied Geophysics*, 111, 203–210. <https://doi.org/10.1016/j.jappgeo.2014.10.009>
- Artiola, J. F., & Brusseau, M. L. (2019). Environmental and pollution science (Third Edition) 2019, Chapter 10-The role of environmental monitoring in pollution science, 149–162. <https://doi.org/10.1016/B978-0-12-814719-1.00010-0>
- Badesab, F., von Döbeneck, T., Bryan, K. R., Müller, H., Briggs, R. M., Frederichs, T., & Kwohl, E. (2012). Formation of magnetite-enriched zones in and offshore of a mesotidal estuarine lagoon: An environmental magnetic study of Tauranga Harbor and Bay of Plenty, New Zealand. *Geochemistry, Geophysics, Geosystems*. <https://doi.org/10.1029/2012gc004125>
- Bao, L. J., Hu, C. F., Hui, C. J., Sheng, X. D., & Hai, X. Q. (2011). Humid Medieval warm period recorded by magnetic characteristics of sediments from Gonghai Lake, Shanxi, North China. *Chinese Science Bulletin*, 56, 2464–2474.
- Bennett, J. D., Cameon, N. R., Bride, D. M. C., Clarke, M. C. G., Djunuddin, A., Ghazali, S. A., Harahap, H., Jeffry, D. H., Kartawa, W., Keats, W., Ngabito, H., Rock, N. M. S., Thompson, S. J. (1983): Peta geologi lembar Banda Aceh, Sumatera, skala 1:250.000. Center for Geological Research and Development. Bandung.
- Biedermann, A. R., Pettke, T., Bender Koch, C., & Hirt, A. M. (2015). Magnetic anisotropy in clinopyroxene and orthopyroxene single crystals. *Journal of Geophysical Research: Solid Earth*, 120(3), 1431–1451. <https://doi.org/10.1002/2014jb011678>
- Burchard, H., Schuttelaar, H. M., & Ralston, D. K. (2018). Sediment trapping in estuaries. *Annual Review of Marine Science*, 10(1), 371–395. <https://doi.org/10.1146/annurev-marine-010816-060535>
- Canbay, M., Aydin, A., & Kurtulus, C. (2010). Magnetic susceptibility and heavy-metal contamination in topsoils along the Izmit Gulf coastal area and IZAYTAS (Turkey). *Journal of Applied Geophysics*, 70(1), 46–57. <https://doi.org/10.1016/j.jappgeo.2009.11.002>
- Chandrasekaran, S., Sankaran Pillai, G., & Venkatraman, B. (2020). Spatial and heavy metal assessment in beach sands of east coast of Tamil Nadu India. *Environmental Nanotechnology, Monitoring & Management*. <https://doi.org/10.1016/j.enmm.2020.100324>
- Chen, Z., Kostaschuk, R., & Yang, M. (2001). Heavy metals on tidal flats in the Yangtze Estuary. *China Environmental Geology*, 40(6), 742–749. <https://doi.org/10.1007/s002540000241>
- Chu, B., Chen, X., Li, Q., Yang, Y., Mei, X., He, B., He, Y., Hui, L., & Tan, L. (2014). Effects of salinity on the transformation of heavy metals in tropical estuary wetland soil. *Chemistry and Ecology*, 31(2), 186–198. <https://doi.org/10.1080/02757540.2014.917174>
- De Souza Machado, A. A., Spencer, K., Kloas, W., Toffolon, M., & Zarfl, C. (2016). Metal fate and effects in estuaries: A review and conceptual model for better understanding of toxicity. *Science of the Total Environment*, 541, 268–281. <https://doi.org/10.1016/j.scitotenv.2015.09.045>
- Dearing, J. A. (1999). Environmental magnetic susceptibility: Using the Bartington MS2 System. Chi Pub, Kenilworth.
- Dessai, D. V. G., Nayak, G. N., & Basavaiah, N. (2009). Grain size, geochemistry, magnetic susceptibility: Proxies in identifying sources and factors controlling distribution of metals in a tropical estuary, India. *Estuarine, Coastal and Shelf Science*, 85(2), 307–318. <https://doi.org/10.1016/j.eccs.2009.08.020>
- Esteller, M. V., Kondratenko, N., Expósito, J. L., Medina, M., & Martín del Campo, M. A. (2017). Hydrogeochemical characteristics of a volcanic-sedimentary aquifer with special emphasis on Fe and Mn content: A case study in Mexico. *Journal of Geochemical Exploration*, 180, 113–126.
- Fabre, S., Jeandel, C., Zambardi, T., Roustan, M., & Almar, R. (2019). An overlooked silica source of the modern oceans:

Are sandy beaches the key? *Frontiers in Earth Science*. <https://doi.org/10.3389/feart.2019.00231>

Fujimori, T., & Takigami, H. (2013). Pollution distribution of heavy metals in surface soil at an informal electronic-waste recycling site. *Environmental Geochemistry and Health*, 36(1), 159–168. <https://doi.org/10.1007/s10653-013-9526-y>

Hamdan, A. M., Bijaksana, S., Tjoa, A., Dahrin, D., & Kirana, K. H. (2019). Magnetic characterizations of nickel hyperaccumulating plants (*Planchonella oxyhedra* and *Rinorea bengalensis*) from Halmahera. *Indonesia. International Journal of Phytoremediation*. <https://doi.org/10.1080/15226514.2018.1524839>

Hamdan, A. M., Bijaksana, S., Tjoa, A., Dahrin, D., Fajar, S. J., & Kirana, K. H. (2020). Use and validation of magnetic properties for differentiating nickel hyperaccumulators and non-nickel hyperaccumulators in ultramafic regions. *Journal of Geochemical Exploration*. <https://doi.org/10.1016/j.gexplo.2020.106581>

Haris, H., Looi, L. J., Aris, A. Z., Mokhtar, N. F., Ayob, N. A. A., Yusoff, F. M., Salleh, A. B., & Praveena, S. M. (2017). Geo-accumulation index and contamination factors of heavy metals (Zn and Pb) in urban river sediment. *Environmental Geochemistry and Health*, 39(6), 1259–1271. <https://doi.org/10.1007/s10653-017-9971-0>

Hopwood, M. J., Statham, P. J., Skrabal, S. A., & Willey, J. D. (2015). Dissolved iron(II) ligands in river and estuarine water. *Marine Chemistry*, 173, 173–182. <https://doi.org/10.1016/j.marchem.2014.11.004>

Jin, B., Wang, M., Yue, W., Zhang, L., & Wang, Y. (2019). Heavy mineral variability in the Yellow River sediments as determined by the multiple-window strategy. *Minerals*, 9(2), 85. <https://doi.org/10.3390/min9020085>

Jilbert, T., Asmala, E., Schröder, C., Tiihonen, R., Myllykangas, J. -P., Virtasalo, J. J., Kotilainen, A., Peltola, P., Ekholm, P., & Hietanen, S. (2018). Impacts of flocculation on the distribution and diagenesis of iron in boreal estuarine sediments. *Biogeosciences*, 15, 1243–1271. <https://doi.org/10.5194/bg-15-1243-2018>

Kanu, M. O., Meludu, O. C., & Oniku, S. A. (2014). Comparative study of topsoil magnetic susceptibility variation based on some human activities. *Geofísica Internacional*, 53(4), 411–423. [https://doi.org/10.1016/s0016-7169\(14\)70075-3](https://doi.org/10.1016/s0016-7169(14)70075-3)

Kowalska, J. B., Skiba, M., & Maj-Szeliga, K. (2021). Does calcium carbonate influence clay mineral transformation in soils developed from slope deposits in Southern Poland? *Journal of Soils and Sediments*, 21, 257–280. <https://doi.org/10.1007/s11368-020-02764-3>

Kumar, R., Srivastava, P. K., & Srivastava, S. P. (1994). Leaching of heavy metals (Cr, Fe, and Ni) from stainless steel utensils in food simulants and food materials. *Bulletin of Environmental Contamination and Toxicology*. <https://doi.org/10.1007/bf00192042>

Kumari, S., Amit, Jamwal, R., Mishra, N., & Singh, D. K. (2020). Recent developments in environmental mercury bioremediation and its toxicity: A review. *Environmental Nanotechnology, Monitoring & Management*, 100283. <https://doi.org/10.1016/j.enmm.2020.100283>

Labrada-Delgado, G., Aragon-Pina, A., Campos-Ramos, A., Castro-Romero, T., Amador-Munoz, O., & Villalobos-Pietrini, R. (2012). Chemical and morphological characterization of PM2.5 collected during MILAGRO campaign using scanning electron microscopy. *Atmospheric Pollution Research*, 3(3), 289–300. <https://doi.org/10.5094/apr.2012.032>

Li, M., Zhu, S., Ouyang, T., Tang, J., & He, C. (2020). Magnetic fingerprints of surface sediment in the Bohai Sea, China. *Marine Geology*, 106226. <https://doi.org/10.1016/j.margeo.2020.106226>

Mariyanto, M., Amir, M. F., Utama, W., Hamdan, A. M., Bijaksana, S., Pratama, A., Yunginger, R., & Sudarningsih, S. (2019). Heavy metal contents and magnetic properties of surface sediments in volcanic and tropical environments from Brantas River, Jawa Timur Province, Indonesia. *Science of the Total Environment*. <https://doi.org/10.1016/j.scitotenv.2019.04.244>

Meng, W., Qin, Y., Zheng, B., & Zhang, L. (2008). Heavy metal pollution in Tianjin Bohai Bay, China. *Journal of Environmental Sciences*, 20(7), 814–819. [https://doi.org/10.1016/s1001-0742\(08\)62131-2](https://doi.org/10.1016/s1001-0742(08)62131-2)

Moechtar, H., Subiyanto, S., & Sugiarto, D. (2009). Geologi Aluvium dan Karakter Endapan Pantai/Pematang Pantai di Lembah Krueng Aceh, Aceh Besar (Provinsi. Nanggroe Aceh Darussalam). *Journal of Geology and Mineral Resources*, 19(4).

Monteil, C. L., Benzerara, K., Menguy, N., Bidaud, C. C., Michot-Achdjian, E., Bolzoni, R., Mathon, F. P., Coutaud, M., Alonso, B., Garau, C., Jézéquel, D., Viollier, E., Ginot, N., Floriani, M., Swaraj, S., Sachse, M., Busigny, V., Duprat, E., Guyot, F., & Lefevre, C. T. (2020). Intracellular amorphous Ca-carbonate and magnetite biomineralization by a magnetotactic bacterium affiliated to the Alphaproteobacteria. *The ISME Journal: Multidisciplinary Journal of Microbial Ecology*. <https://doi.org/10.1038/s41396-020-00747-3>

Nakanishi, R., Baba, A., Tsuyama, T., Ikemi, H., & Mitani, Y. (2019). Examination of sediment dynamics based on the distribution of silica fluxes and flood sediments in the Otoishi River related to the Northern Kyushu heavy rain disaster, July 2017. *Geosciences*, 9(2), 75. <https://doi.org/10.3390/geosciences9020075>

Naseh, M. R. V., Karbassi, A., Ghazaban, F., Baghvand, A., & Mohammadzadeh, M. J. (2012). Magnetic susceptibility as a proxy to heavy metal content in the sediments of Anzali wetland, Iran. *Iranian Journal of Environmental Health Science & Engineering*, 9(1), 34. <https://doi.org/10.1186/1735-2746-9-34>

Novala, G. C., Fitriani, D., Susanto, K., & Kirana, K. H. (2016). Magnetic properties of soils from Sarimukti landfill as proxy indicators of pollution (Case Study: Desa Sarimukti, Kabupaten Bandung Barat). *IOP Conference Series: Earth and Environmental Science*, 29, 1–6. <https://doi.org/10.1088/1755-1315/29/1/012015>

Oldham, V. E., Miller, M. T., Jensen, L. T., & Luther, G. W. (2017). Revisiting Mn and Fe removal in humic rich estuaries. *Geochimica Et Cosmochimica Acta*, 209, 267–283. <https://doi.org/10.1016/j.gca.2017.04.001>

Peter, P. O., Rashid, A., Hou, L., Nkinahamira, F., Kiki, C., Sun, Q., Yu, C. P., & Hu, A. (2020). Elemental contaminants in surface sediments from Jiulong River Estuary, China: Pollution level and ecotoxicological risk assessment. *Water*, 12(6), 1640. <https://doi.org/10.3390/w12061640>

- Priya, K. L., Jegathambal, P., & James, E. J. (2016). Salinity and suspended sediment transport in a shallow estuary on the east coast of India. *Regional Studies in Marine Science*, 7, 88–99. <https://doi.org/10.1016/j.rsma.2016.05.015>
- Reitermajer, D., Celino, J. J., & Queiroz, A. F. D. S. (2011). Heavy metal distribution in the sediment profiles of the Sauípe River Estuary, north seashore of the Bahia State, Brazil. *Microchemical Journal*, 99(2), 400–405. <https://doi.org/10.1016/j.microc.2011.06.015>
- Reyes, A. B., Bautista, F., Goguitchaichvili, A., Contreras, A. J. J., Battu, J., Quintana Owen, P., & Carvallo, C. (2013). Rock-magnetic properties of topsoils and urban dust from Morelia (>800,000 inhabitants), Mexico: Implications for anthropogenic pollution monitoring in Mexico's medium size cities. *Geofísica Internacional*, 52(2), 121–133. [https://doi.org/10.1016/s0016-7169\(13\)71467-3](https://doi.org/10.1016/s0016-7169(13)71467-3)
- Sudarningsih, S., Bijaksana, S., Hafidz, A., Pratama, A., Widodo, W., Iskandar, I., Dahrin, D., Fajar, S. J., & Santoso, N. A. (2017). Variations in the concentration of magnetic minerals and heavy metals in suspended sediments from Citarum River and its tributaries, West Java. *Indonesia. Geosciences*, 7(3), 66. <https://doi.org/10.3390/geosciences7030066>
- Togibasa, O., Bijaksana, S., & Novala, G. (2018). Magnetic properties of iron sand from the Tor River Estuary, Sarmi, Papua. *Geosciences*, 8(4), 113. <https://doi.org/10.3390/geosciences8040113>
- Wu, J., Liu, J. T., & Wang, X. (2012). Sediment trapping of turbidity maxima at the Changjiang estuary. *Marine Geology*, 303–306, 14–25. <https://doi.org/10.1016/j.margeo.2012.02.011>
- Xu, Q., Xing, R., Sun, M., Gao, Y., & An, L. (2020). Microplastics in sediments from an interconnected river-estuary region. *Science of the Total Environment*, 729, 139025. <https://doi.org/10.1016/j.scitotenv.2020.139025>
- Yang, L., Song, X., Zhang, Y., & Han, D. (2012). Characterizing interactions between surface water and groundwater in the Jialu River basin using major ion chemistry and stable isotopes. *Hydrology and Earth System Sciences*, 9(5), 5955–5981.
- Yi, Q., Dou, X. D., Huang, Q. R., & Zhao, X. Q. (2012). Pollution characteristics of Pb, Zn, As, Cd in the Bijiang River. *Procedia Environmental Sciences*, 13, 43–52. <https://doi.org/10.1016/j.proenv.2012.01.004>
- Yunginger, R., Bijaksana, S., Dahrin, D., Zulaikah, S., Hafidz, A., Kirana, K., & Fajar, S. (2018). Lithogenic and anthropogenic components in surface sediments from Lake Limboto as shown by magnetic mineral characteristics, trace metals, and REE geochemistry. *Geosciences*, 8(4), 116. <https://doi.org/10.3390/geosciences8040116>
- Zhao, G., Ye, S., Yuan, H., Ding, X., & Wang, J. (2016). Surface sediment properties and heavy metal pollution assessment in the Pearl River Estuary, China. *Environmental Science and Pollution Research*, 24(3), 2966–2979. <https://doi.org/10.1007/s11356-016-8003-4>
- Zhu, X., Zhang, R., Wu, Y., Zhu, J., Bao, D., & Zhang, J. (2018). The remobilization and removal of Fe in estuary-A case study in the Changjiang Estuary, China. *Journal of Geophysical Research: Oceans*, 123(4), 2539–2553. <https://doi.org/10.1002/2017jc013671>

Publisher's Note Springer Nature remains neutral with regard to jurisdictional claims in published maps and institutional affiliations.